Anisotropic scattering rates and antiferromagnetic precursor effects in the t-t'-U Hubbard model

J. Altmann, W. Brenig, Arno P. Kampf

Angaben zur Veröffentlichung / Publication details:

Altmann, J., W. Brenig, and Arno P. Kampf. 2000. "Anisotropic scattering rates and antiferromagnetic precursor effects in the t-t'-U Hubbard model." *European Physical Journal B* 18 (3): 429–33. https://doi.org/10.1007/s100510070029.

Anisotropic scattering rates and antiferromagnetic precursor effects in the t-t′-U Hubbard model

J. Altmann[1], W. Brenig[2], and A.P. Kampf[3,a]

[1] Institut für Theoretische Physik, Universität zu Köln, Zülpicher Str. 77, 50937 Köln, Germany
[2] Institut für Theoretische Physik, Technische Universität Braunschweig, 38106 Braunschweig, Germany
[3] Institut für Physik, Theoretische Physik III, Universität Augsburg, 86135 Augsburg, Germany

Abstract. We have investigated the evolution of the electronic properties of the t-t'-U Hubbard model with hole doping and temperature. Due to the shape of the Fermi surface, scattering from short wavelength spin fluctuations leads to strongly anisotropic quasi–particle scattering rates at low temperatures near half–filling. As a consequence, significant variations with momenta near the Fermi surface emerge for the spectral functions and the corresponding ARPES signals. At low doping the inverse lifetime of quasiparticles on the Fermi surface is of order $k_{\rm B}T$ varying linearly in temperature from energies of order t down to a very low energy scale set by the spin fluctuation frequency while at intermediate doping a sub-linear T-dependence is observed. This behavior is possibly relevant for the interpretation of photoemission spectra in cuprate superconductors at different hole doping levels.

PACS. 74.72.-h High-T_c compounds – 75.50.Ee Antiferromagnetics – 79.60.-i Photoemission and photoelectron spectra

1 Introduction

A key issue in the efforts to understand the microscopic physics of high–$T_{\rm c}$ superconductors is the evolution of the electronic properties with doping. In recent years theoretical work has continuously benefited from angular resolved photoemission spectroscopy (ARPES) data for the electronic spectrum and the Fermi surface (FS) in the normal state as well as for the anisotropic energy gap in the superconducting state [1]. In particular, remarkable ARPES results for the underdoped cuprates have shown an anisotropic normal–state pseudogap which forms below ~ 150 K for the weakly underdoped materials increasing up to ~ 300 K for the heavily underdoped compounds with a $T_{\rm c}$ close to zero [2–5]. Even for optimally doped Bi 2212 samples pseudogap formation has been reported near the $(\pi,0)$ point of the Brillouin zone (BZ) [6]. Contrary to overdoped samples the quasi–particle (qp) peak in the underdoped spectra is found to be very weak near the $(\pi,0)$ point of the BZ and no FS crossing is observed on the BZ boundary along the $(\pi,0)$ to (π,π) direction which has been considered as evidence for the destruction of the FS [7]. Very recent high resolution ARPES studies have also convincingly demonstrated the previously anticipated linear temperature dependence of the inverse lifetime of the excitations along the BZ diagonal [8].

Furthermore, the spin susceptibility [9], c–axis optical [10] as well as in–plane infrared conductivity [11], NMR relaxation rates [12], and inelastic neutron scattering data [13] indicate a pseudogap in the low–energy excitation spectrum of underdoped compounds. Different scenarios like pair formation well above $T_{\rm c}$ [14,15], spin–charge separation [16,17] or precursor effects near the antiferromagnetic (AF) instability [18,19] have been proposed as possible origins of these pseudogap phenomena.

Some of the observed features like the appearance of anomalously flat bands near the Fermi energy [20] have been previously discussed in the context of the t-J model Hamiltonian. The necessity to include longer range hopping processes was recognized in direct comparisons of ARPES dispersions and t-J model spectra [21,22]. *E.g.* a next–nearest neighbor hopping amplitude was found crucial to obtain a weak qp weight near the $(\pi,0)$ point of the BZ [23,24].

In this paper, we explore the combined effects of strong spin fluctuation scattering and FS topology using the 2D Hubbard model on a square lattice with a $t-t'$ dispersion of the one-particle kinetic energy

$$\epsilon_{\mathbf{k}} = -2t(\cos k_x + \cos k_y) - 4t' \cos k_x \cos k_y \qquad (1)$$

with nearest–neighbor (t) and next–nearest neighbor (t') hopping amplitudes. Near half–filling we demonstrate that strong qp scattering rates develop with decreasing temperature near the so called "hot spots" on the FS, *i.e.* FS points which are connected by the AF wave vectors $\mathbf{Q} = (\pm\pi, \pm\pi)$. As a consequence of the emerging highly anisotropic scattering rates the qp peaks in the spectral

[a] e-mail: kampfa@physik.uni-augsburg.de

functions near the $(\pi, 0)$ points of the BZ are suppressed in comparison to the momenta near $\mathbf{k}_{\rm F}$ along the BZ diagonal leading to highly anisotropic ARPES signals. In this regime the imaginary part of the on-shell self-energy is of order $k_{\rm B}T$ and is varying linearly with temperature down to the very low energy scale set by the spin fluctuation frequency. Simultaneously, a pseudogap develops in the density of states (DOS) whose width is controlled by the magnitude of t'.

2 FLEX approximation

Our method of choice to evaluate the renormalized one-particle excitations is the self–consistent and conserving [25] fluctuation–exchange (FLEX) approximation [26]. In this approach the self–energy is given in terms of the spin– and density–fluctuation T–matrices $T_{\rm sf}(\mathbf{r}, \tau)$ and $T_{\rho\rho}(\mathbf{r}, \tau)$ by

$$\Sigma(\mathbf{r}, \tau) = U^2 G(\mathbf{r}, \tau)[\chi_0(\mathbf{r}, \tau) + T_{\rho\rho}(\mathbf{r}, \tau) + T_{\rm sf}(\mathbf{r}, \tau)] \quad (2)$$

where $\chi_0(\mathbf{r}, \tau) = -G(\mathbf{r}, \tau)G(-\mathbf{r}, -\tau)$ is the particle–hole bubble and $\mathbf{r}$ and τ denote the real space coordinate and imaginary time, respectively. U is the on–site Coulomb repulsion. The Fourier transformed T-matrices are

$$T_{\rho\rho}(\mathbf{q}, \mathrm{i}\omega_m) = -\frac{1}{2}\frac{U\chi_0^2(\mathbf{q}, \mathrm{i}\omega_m)}{1 + U\chi_0(\mathbf{q}, \mathrm{i}\omega_m)} \quad (3)$$

$$T_{\rm sf}(\mathbf{q}, \mathrm{i}\omega_m) = \frac{3}{2}\frac{U\chi_0^2(\mathbf{q}, \mathrm{i}\omega_m)}{1 - U\chi_0(\mathbf{q}, \mathrm{i}\omega_m)} \quad (4)$$

where $\omega_m = 2m\pi T$ are the bosonic Matsubara frequencies at temperature T. In combination with Dyson's equation $G^{-1} = G_0^{-1} - \Sigma$, equations (1, 2), and (3) form a self–consistent set of equations which we solve numerically by iteration. This numerical solution is based on a completely algebraic treatment using repeated application of intermediate Fast–Fourier–transforms [27]. Stability of the self–consistent cycle is achieved by solving the FLEX equations on a contour in the complex frequency plane shifted off the real axis by a finite amount $\mathrm{i}\gamma$ with $0 < \gamma < \pi T/2$ [29]. Analytic continuation to the real frequency axis does not encounter the usual problems of purely imaginary frequency methods [27].

We have solved the FLEX equations on lattices with up to 128×128 sites using an equally spaced frequency mesh of 4096 points within an energy window of $[-30t, 30t]$. The lower bound on the temperature accessible in our present calculations is $T \sim 0.02t$. This bound is set by the smallest width in frequency space of the AF paramagnon–peak in Im $T_{\rm sf}(\mathbf{q}, \omega + \mathrm{i}\gamma)$ which can be resolved for the chosen frequency mesh and the smallest momentum space width which can be treated without introducing finite size effects. Throughout the paper we will adopt an interaction strength $U = 4t$ and $t' = -0.3t$ – a parameter set for which the model exhibits long range AF order in the ground state at half–filling [28].

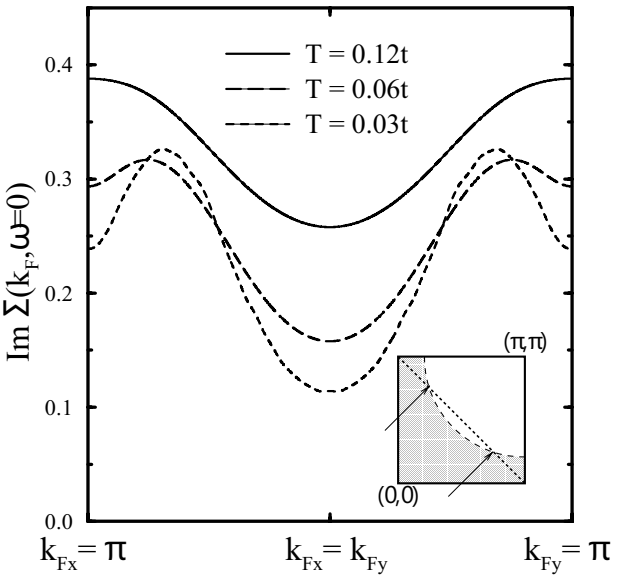

Fig. 1. Im $\Sigma(\mathbf{k}_{\rm F}, \omega = 0)$ along the Fermi line for various temperatures T with $U = 4t$, $t' = -0.3t$ and hole doping $\delta = 2.5\%$. The inset shows schematically the Fermi line (long dashed line) in one quarter of the BZ and the "hot spots" are indicated by arrows.

3 Scattering rates and spectral functions

We start with the discussion of our results by considering the FS anisotropy of the one-particle scattering rate for small hole concentrations. Its momentum dependence is governed by two effects: First, the available recoil phase–space which is linked to the momentum–space width of the AF paramagnon peak in Im $T_{\rm sf}(\mathbf{q}, \omega)$ and second the density of intermediate states. While the former quantity exhibits a variation with temperature and doping which discriminates only weakly between the t– and the t–t' model in the low doping limit, the latter quantity depends crucially on the t–t' band structure. This is a major source of difference between the one-particle renormalizations in the t– and t–t' Hubbard models. In particular, we observe a non–trivial temperature and momentum dependence of the self–energy. This is shown in Figure 1 which depicts the imaginary part of $\Sigma(\mathbf{k}, \omega = 0)$ along the FS line, *i.e.* at $\mathbf{k} = \mathbf{k}_{\rm F}$. For $T \geq 0.08t$ the AF peak in Im $T_{\rm sf}(\mathbf{q}, \omega)$ is a broad structure; its HWFMs in momentum and frequency space are $\sim \pi/6$ and $\sim 0.2t$, respectively. Therefore, in essence, $\Sigma(\mathbf{k}_{\rm F}, \omega = 0)$ is modulated only by the density of states along the FS which is largest at the borders of the BZ and smallest at the point $\mathbf{k}_{{\rm F}\gamma}$ on the BZ diagonal, *i.e.* where $k_{{\rm F}x} = k_{{\rm F}y}$. For decreasing temperatures the peak in Im $T_{\rm sf}(\mathbf{q}, \omega)$ at $\mathbf{q} = \mathbf{Q}$ sharpens until we loose its accurate resolution at about $T \approx 0.02t$. This redistribution of weight shifts the maximum in Im $\Sigma(\mathbf{k}_{\rm F}, \omega = 0)$ into the so–called "hot spots" on the FS which can be connected by the AF wave vectors. In addition to this shift the low–temperature anisotropy of the self–energy is enhanced by roughly a factor of two.

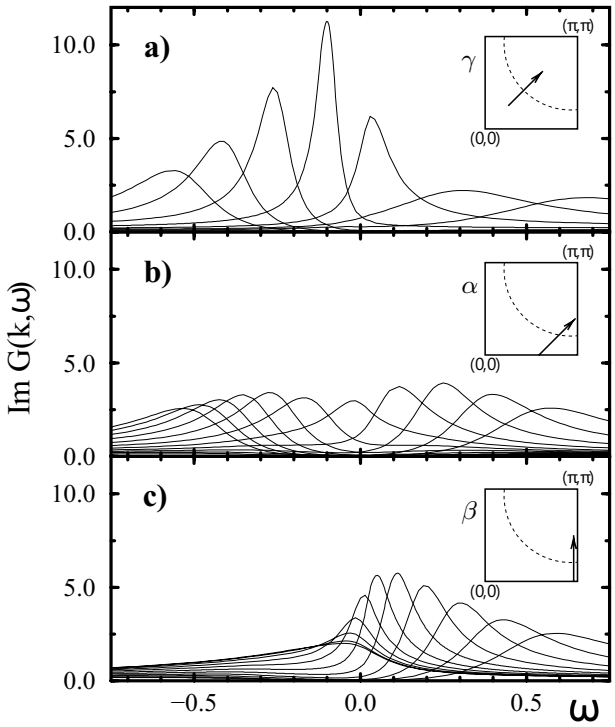

Fig. 2. Im $G(\mathbf{k},\omega)$ along three different paths in the BZ – schematically shown in the insets – for $T = 0.03t$, $U = 4t$, $t' = -0.3t$ and $\delta = 2.5\%$ on a 64×64 lattice. The path γ in (a) is chosen along the BZ diagonal from $\mathbf{k}_\gamma = (11,11)\frac{\pi}{32}$ to $(17,17)\frac{\pi}{32}$. In (b) the path α is parallel to the path in (a) but runs from $\mathbf{k}_\alpha = (21,0)\frac{\pi}{32}$ to $(32,11)\frac{\pi}{32}$ crossing the hot spot at $\mathbf{k}_{\mathrm{F}\alpha} \approx (26,5)\frac{\pi}{32}$. The path β in (c) is along the BZ boundary from $\mathbf{k}_\beta = (32,0)\frac{\pi}{32}$ to $(32,11)\frac{\pi}{32}$.

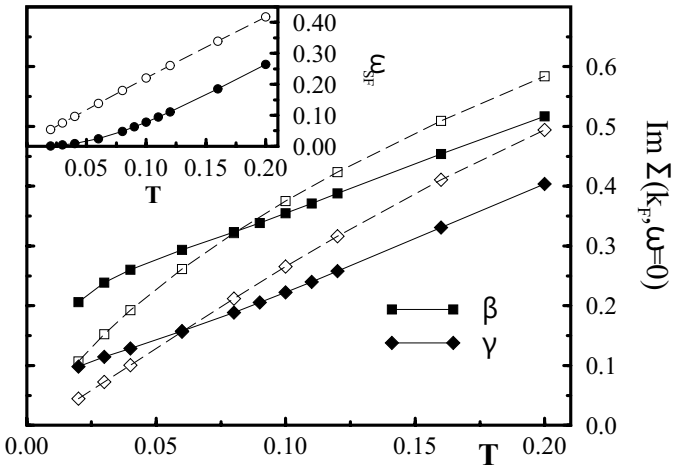

Fig. 3. Temperature dependence of Im $\Sigma(\mathbf{k}_\mathrm{F},\omega=0)$ for two momenta on the Fermi line ($\mathbf{k}_{\mathrm{F}\beta}$ at the border of the BZ, and $\mathbf{k}_{\mathrm{F}\gamma}$ along the diagonal; $U = 4t$, and $t' = -0.3t$). The inset displays the temperature dependence of the spin fluctuation energy ω_{sf}. Filled symbols/solid lines show the results for $\delta = 2.5\%$, open symbols/dashed lines for $\delta = 15\%$.

In Figure 2 we show the consequence of the anisotropic scattering rates for the single–particle spectral function Im $G(\mathbf{k},\omega)$ at $T = 0.03t$. Choosing a path in momentum space as shown in Figure 2a which crosses the FS at $\mathbf{k}_{\mathrm{F}\gamma}$, *i.e.* the wave vector of the minimal scattering rate, a sharp qp peak is observed. In contrast, the qp feature appears severely weakened in Figure 2b where the FS is traversed by passing through a hot spot. In comparison to Figure 2a the amplitude of the qp peak near $\mathbf{k}_\mathrm{F}$ is reduced by almost a factor of three and, moreover, it is *minimal on the FS*. Choosing a path which cuts the FS on the BZ boundary as in Figure 2c, the qp structure is asymmetrically distributed as a function of momentum and more pronounced in the inverse photoemission sector. Only weak dispersion of the qp peak below the Fermi energy along this cut signals a "flat–band" region close to the momentum $(\pi,0)$. We note that ARPES spectra can be obtained from Figures 2a–2c by multiplying Im $G(\mathbf{k},\omega)$ with the Fermi function. It is only near momentum $\mathbf{k}_{\mathrm{F}\gamma}$ where these spectra display sharp qp peaks while the weight of the qp in the vicinity of the hot spots and the BZ boundary is substantially reduced.

Figure 3 summarizes the temperature dependence of the imaginary part of the on–shell ($\omega = 0$) self–energy at the FS for two doping concentrations $\delta = 15\%$ and 2.5% for momenta on the BZ boundary and the BZ diagonal, *i.e.*, $\mathbf{k}_{\mathrm{F}\beta}$ and $\mathbf{k}_{\mathrm{F}\gamma}$, respectively. The inset shows the temperature dependence of the spin fluctuation frequency $\omega_{\mathrm{sf}}(T)$ for both doping concentrations. We define $\omega_{\mathrm{sf}}(T)$ by the frequency of the maximum in Im $T_{\mathrm{sf}}(\mathbf{q},\omega)$ at $\mathbf{q} = \mathbf{Q}$. Figure 3 suggests the existence of a very small energy scale which is manifest in the self–energy at low doping. At $\delta = 15\%$ Im $\Sigma(\mathbf{k}_\mathrm{f},\omega = 0,T)$ clearly extrapolates to zero for vanishing temperatures at both FS momenta. This is consistent with Fermi–liquid theory (FLQ). However, at $\delta = 2.5\%$ a similar behavior is not found. In order to preserve low–temperature FLQ behavior we are forced to assume that Im $\Sigma(\mathbf{k}_\mathrm{f},\omega = 0,T)$ will approach zero below a very low characteristic temperature $T^{\mathrm{FLQ}}(\delta)$. Since $\omega_{\mathrm{sf}}(T)$ is the only low–energy scale available which remains finite in the limit $T \to 0$ for any $\delta > 0$, it is natural to assume that $T^{\mathrm{FLQ}}(\delta) \sim \omega_{\mathrm{sf}}(T^{\mathrm{FLQ}}(\delta))$. As is obvious from the inset of Figure 3b this temperature is very low for $\delta = 2.5\%$ and remains inaccessible within the numerical accuracy of our present computational scheme. However, renormalization group techniques applied the FLEX equations at very low temperatures of order $k_\mathrm{B}T \sim 10^{-4}t$ have confirmed the persistence of FLQ behavior [30] and are consistent with our data and conclusions.

Figure 4 shows the density of states in the vicinity of the Fermi energy at $T = 0.03t$. At this temperature a pseudogap has clearly opened. However, by increasing the magnitude of the next–nearest neighbor hopping amplitude t' the nesting phase-space is reduced and the pseudogap is diminished and eventually disappears. Yet, in the latter case, we find a pseudogap to persist in parts of the BZ, *i.e.* near the $(\pi,0)$ point. This partial pseudogap formation was also pointed out in references [31,32].

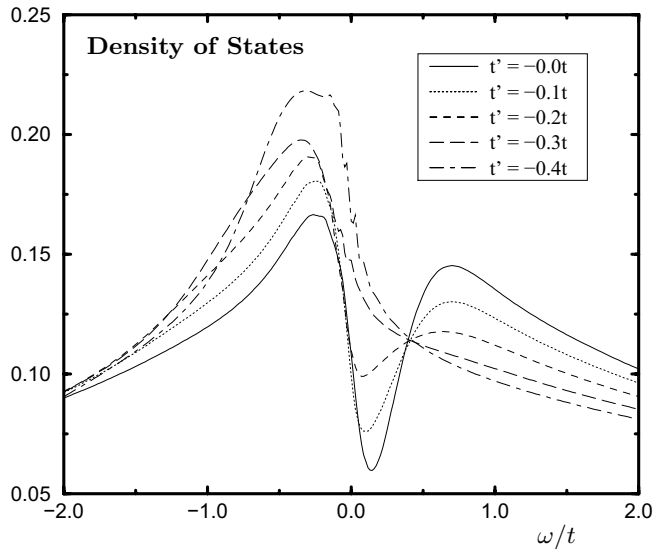

Fig. 4. Density of states in the vicinity of the Fermi energy. Results are shown for $T = 0.03t$, $U = 4t$, and doping $\delta = 5\%$ and various values of t' as indicated in the figure.

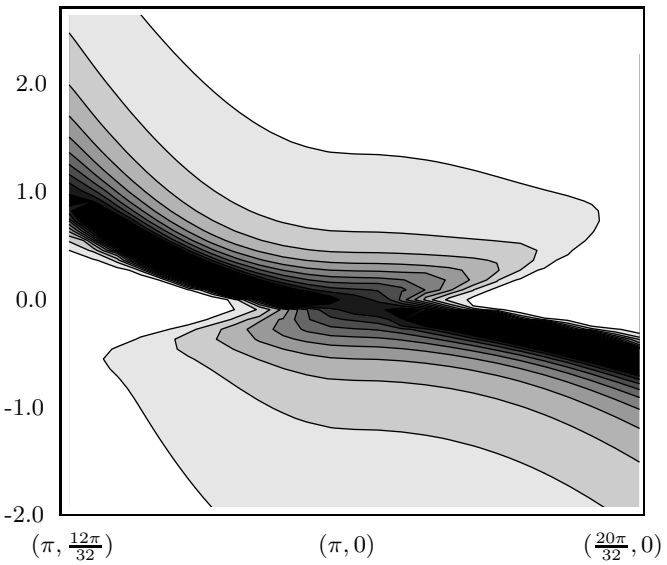

Fig. 5. Density-plot of the spectral function along the path $(\pi, \frac{12\pi}{32}) \rightarrow (\pi, 0) \rightarrow (\frac{20\pi}{32}, 0)$ in the BZ. The parameters are $T = 0.03t, t' = -0.3t, \delta = 2.5\%, U = 4t$.

Figure 5, shows a contour–plot of the dispersion of the one-particle spectral function in a parameter range of relatively strong spin fluctuation scattering. Focusing on the low–energy sector in the vicinity the Fermi level it is evident that the dispersion of the dominant spectral peak is consistent with the notion of a large FS. However, upon crossing the FS the spectral weight of this peak is reduced – as can be seen in the vicinity of the point $(\pi, 0)$ – and the remaining spectral weight is shifted off into AFM precursor bands which extend over some region of the BZ. These results are reminiscent of similar findings in references [31,33] although less pronounced.

4 Summary

In conclusion we have studied the effects of strong spin–fluctuation scattering and the FS shape on the evolution of anisotropic electronic properties of the 2D U-t-t' Hubbard model. With decreasing hole doping a linear temperature dependence of the qp scattering-rate develops in addition to low-temperature FS-hot-spots. This is consistent with several aspects of the ARPES signals in the underdoped cuprates. No signature of a FS collapse is found within FLEX at low doping, where however a pseudogap and AFM precursor band develop.

This research was performed within the program of the SFB 341 of the Deutsche Forschungsgemeinschaft (DFG). A.P.K. acknowledges support through SFB 484.

References

1. For a review see Z.-X. Shen, D. Dessau, Phys. Rep. **253**, 1 (1995).
2. D.S. Marshall, D.S. Dessau, A.G. Loeser, C.-H. Park, A.Y. Matsuura, J.N. Eckstein, I. Bozovic, P. Fournier, A. Kapitulnik, W.E. Spicer, Z.-X. Shen, Phys. Rev. Lett. **76**, 4841 (1996).
3. A.G. Loeser, Z.-X. Shen, D.S. Dessau, D.S. Marshall, C.H. Park, P. Fournier, A. Kapitulnik, Science **273**, 325 (1996).
4. H. Ding, T. Yokoya, J.C. Campuzano, T. Takahashi, M. Randeria, M.R. Norman, T. Mochiku, K. Kadowaki, J. Giapintzakis, Nature **382**, 51 (1996).
5. A. Ino, T. Mizokawa, K. Kobayashi, A. Fujimori, T. Sasagawa, T. Kimura, K. Kishio, K. Tamasaku, H. Eisaki, S. Uchida, Phys. Rev. Lett. **81**, 2124 (1998).
6. N.L. Saini, J. Avila, A. Bianconi, A. Lanzara, M.C. Asensio, S. Tajima, G.D. Gu, N. Koshizuka, Phys. Rev. Lett. **79**, 3467 (1997).
7. M.R. Norman. H. Ding, M. Randeria, J.C. Campuzano, T. Yokoya, T. Takeuchi, T. Takahashi, T. Mochiku, K. Kadowaki, P. Guptasarma, D.G. Hinks, Nature **392**, 157 (1998).
8. T. Valla, A.V. Fedorov, P.D. Johnson, B.O. Wells, S.L. Hulbert, Q. Li, G.D. Gu, N. Koshizuka, Science **285**, 2110 (1999).
9. M. Oda *et al.*, Physica C **183**, 234 (1991).
10. C.C. Homes, T. Timusk, R. Liang, D.A. Bonn, W.N. Hardy, Phys. Rev. Lett. **71**, 1645 (1993).
11. D.N. Basov, R. Liang, B. Dabrowski, D.A. Bonn, W.N. Hardy, T. Timusk, Phys. Rev. Lett. **77**, 4090 (1996); A.V. Puchkov, P. Fournier, D.N. Basov, T. Timusk, A. Kapitulnik, N.N. Kolesnikov, Phys. Rev. Lett. **77**, 3212 (1996).

12. M. Takigawa, A.P. Reyes, P.C. Hammel, J.D. Thompson, R.H. Heffner, Z. Fisk, K.C. Ott, Phys. Rev. B **43**, 247 (1991).
13. J. Rossat–Mignod *et al.*, Physica B **169**, 58 (1991).
14. S. Doniach, M. Inui, Phys. Rev. B **41**, 6668 (1990); Y. Uemura *et al.*, Phys. Rev. Lett. **66**, 2665 (1991); M. Randeria, N. Trivedi, A. Moreo, R.T. Scalettar, Phys. Rev. Lett. **69**, 2001 (1992).
15. V.J. Emery, S.A. Kivelson, Nature **374**, 434 (1995); J. Ranninger, J.-M. Robin, Phys. Rev. B **53**, 11961 (1996); J. Maly *et al.*, Phys. Rev. B **54**, 15657 (1996) and references therein.
16. H. Fukuyama, Prog. Theor. Phys. Suppl. **108**, 287 (1992).
17. X.G. Wen, P. Lee, Phys. Rev. Lett. **76**, 503 (1996).
18. Z.-X. Shen, J.R. Schrieffer, Phys. Rev. Lett. **78**, 1771 (1997).
19. A.V. Chubukov, D. Pines, B.P. Stojkovic, J. Phys. Cond. Matt. **8**, 10017 (1996); D. Pines, *Proceedings of the Euroconference on "Correlations in Unconventional Quantum Liquids", Evora, Portugal, 1996.*
20. E. Dagotto, A. Nazarenko, M. Boninsegni, Phys. Rev. Lett. **73**, 728 (1994).
21. A. Nazarenko, K.J.E. Vos, S. Haas, E. Dagotto, R. Gooding, Phys. Rev. B **51**, 8676 (1995); R. Eder, Y. Ohta, G. Sawatzky, Phys. Rev. B **55**, R3414 (1997).
22. G.B. Martins, R. Eder, E. Dagotto, Phys. Rev. B **60**, R3716 (1999); T. Tohyama, Y. Shibata, S. Maekawa, Z.-X. Shen, N. Nagaosa, J. Phys. Soc. Jpn **69**, 9 (2000).
23. C. Kim, P.J. White, Z.-X. Shen, T. Tohyama, Y. Shibata, S. Maekawa, B.O. Wells, Y.J. Kim, R.J. Birgeneau, M.A. Kastner, Phys. Rev. Lett. **80**, 4245 (1998).
24. For a recent review see T. Tohyama, S. Maekawa, Superconductor Sci. Techn. **13**, 17 (2000).
25. G. Baym, Phys. Rev. **127**, 1391 (1962).
26. N.E. Bickers, D.J. Scalapino, Ann. Phys. (N.Y.) **193**, 206 (1989).
27. J.W. Serene, D.W. Hess, in *Recent Progress in Many–Body Theories*, edited by T.L. Ainsworth *et al.* (Plenum Press, New York, 1992), Vol. 3, and references therein.
28. D. Duffy, A. Moreo, Phys. Rev. B **52**, 15607 (1995).
29. J. Schmalian, M. Langer, S. Grabowski, K.H. Bennemann, Comp. Phys. Commun. **93**, 141 (1996).
30. S. Wermbter, Phys. Rev. B **55**, R10149 (1997).
31. R. Preuss, W. Hanke, C. Gröber, H.G. Evertz, Phys. Rev. Lett. **79**, 1122 (1997).
32. G. Hildebrand, E. Arrigoni, C. Gröber, W. Hanke, Phys. Rev. B **59**, 6534 (1999).
33. D. Duffy, A. Nazarenko, S. Haas, A. Moreo, J. Riera, E. Dagotto, Phys. Rev. B **56**, 5597 (1997).